Saddle Coils for Uniform Static Magnetic Field Generation in NMR Experiments

F. BONETTO,[1] E. ANOARDO,[1] M. POLELLO[2]

[1] *Facultad de Matemática, Astronomía y Física, Universidad Nacional de Córdoba, Ciudad Universitaria, X5016LAE Córdoba, Argentina*
[2] *Stelar s.r.l., Mede (PV), Italy*

ABSTRACT: The magnetic flux density field (called, henceforth, "magnetic field," for the sake of simplicity) generated by a saddle coil system is numerically calculated in the whole space and experimentally tested in two different spatial planes. The uniformity of the magnetic field is studied using Taylor series expansions of the three components separately. The optimum geometry is revised and obtained from the second-order Taylor expansions. The most favorable relationship between saddle coil geometric parameters is determined in case the optimum geometry cannot be achieved (because of experimental restrictions). Approximated manipulable analytical expressions are obtained via fourth-order Taylor expansions of the three components of the magnetic field and compared with exact expressions. They were found to differ in less than 10^{-3}% within a sample region, when typical sample and coil dimensions are considered. Deviations of the magnetic field produced by an optimum-compensating saddle coil system were contrasted with typical NMR field-cycling magnetic field inhomogeneities. Possible influences of such deviations in NMR experiments are discussed. Concepts Magn Reson Part B (Magn Reson Engineering) 29B: 9–19, 2006

KEY WORDS: saddle coils; magnetic field uniformity; field-cycling NMR

INTRODUCTION

The problem of setting up a uniform magnetic field within a given space volume has been treated in different contexts. In nuclear magnetic resonance (NMR) applications, high-resolution experiments usually demand field homogeneities of a few ports per million within a space volume of 0.5 cm^3. In general, depending on the specific application, requirements may be posed on a larger volume or may be more or less flexible with respect to the maximum allowed magnetic field deviations. To assess these issues, additional zonal and tesseral shim coils may be used to add corrections up to the fifth or higher order in the Taylor's expansion of the field gradient (*1–10*). One area of interest concerns the compensation of static external field contributions within a (sample) volume of about a cubic centimeter, where the axial component can be partially compensated by the NMR magnet itself (the remaining part of this axial component can be compensated by the implementation of a suitable Helmholtz coil system).

The need for compensating external contributions from the environment becomes critical in NMR field-cycling experiments (*11*), especially when the relevant evolution of the spin system occurs at low fields of the residual contributions from the environment (earth's field, other magnets in the lab, strong iron pieces, and so on) (*12*). Among other techniques, the

Received 5 March 2005; revised 19 August 2005; accepted 11 October 2005

Correspondence to: Dr. Fernando Bonetto; E-mail: bonetto@famaf.unc.edu.ar

Concepts in Magnetic Resonance Part B (Magnetic Resonance Engineering), Vol. 29B(1) 9–19 (2006)

Published online in Wiley InterScience (www.interscience.wiley.com). DOI 10.1002/cmr.b.20057

problem is intrinsic in zero-field spectroscopy, nuclear quadrupole double resonance, and low-field NMR relaxometry (*11, 13*).

The compensation field can be implemented through external coils arranged around the volume space of interest. When the geometry of the system is cylindrical, saddle coils can easily be adapted, as they are of simple construction. To ensure the magnetic field is uniform within a given space volume, it is imperative to have a clear understanding of the optimal configuration of the compensating coils. It is also important to understand how the currents in a coil bridge can be unbalanced in order to introduce controlled compensating gradients. For a clear understanding of the problem, we need to understand the solution in the whole space and for all the components of the field.

The problem of calculating the optimum geometry of saddle-shaped coils has been addressed by Ginsberg et al. (*14*). In this work, however, the authors deal only with the local magnetic field uniformity within a space volume around the geometric center of the coil system, while focusing in the main field component. Because we are more interested in the magnetic field uniformity in a larger volume and in all directions, we calculated the generated magnetic field exactly in the whole space and compared it with the fourth-order Taylor expansions of the three components of the magnetic field. The homogeneity of magnetic fields produced by saddle coils systems with different geometric configurations was also analyzed.

RESULTS

Calculus of the Magnetic Field

A saddle coil system can be constructed by crushing two equal rectangular coils on a cylindrical shell (see Fig. 1). The same current is carried by each coil, and the direction of the flowing current may be set in Helmholtz or anti-Helmholtz configuration. It is well known that a uniform magnetic field in a given direction can be produced using the former configuration (*14*), and the second one is widely used to produce linear field gradients (*15, 16*).

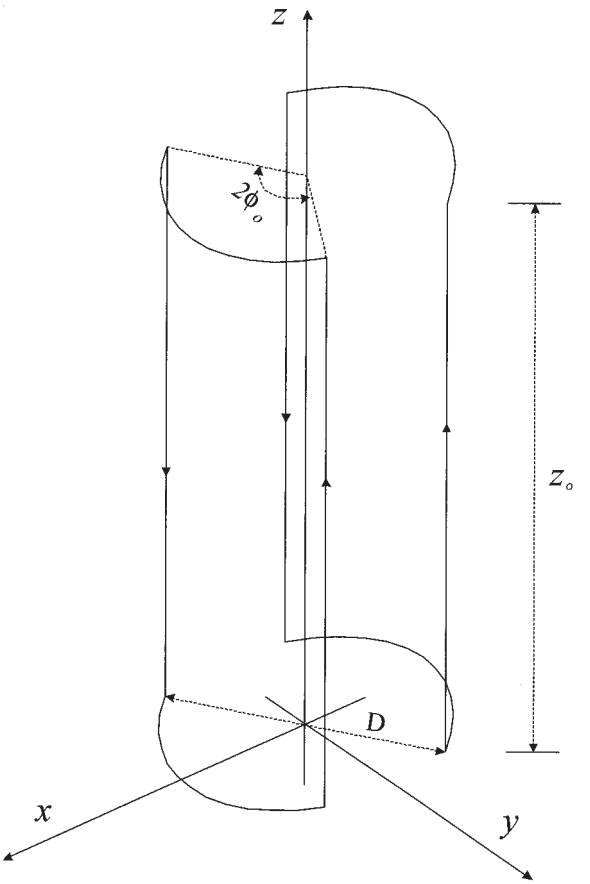

Figure 1 Saddle coil geometry and the coordinate system used.

To calculate the magnetic field anywhere in the space produced by a saddle coil with an aperture angle $2\phi_o$, height z_o, and radius R ($R = D/2$, D being the diameter of the coil), the Biot-Savart law (*17*) was applied to each of the four arcs and strips of the arrangement. All the geometric parameters and the selected coordinate system are specified in Fig. 1. The origin of the coordinate system coincides with the geometric center of the bottom circular region determined by the coil's arcs (see Fig. 1). For the Helmholtz configuration, the magnetic fields $\vec{B}_{ar1}$ and $\vec{B}_{st1}$ produced by the arc situated in the bottom of the coil (in the x direction) and the strip located in the first quadrant of the x–y plane, respectively, are given by (*17*):

$$\overrightarrow{B_{ar1}}(\rho, \phi, z) = \frac{\mu_o}{4\pi} NRI \int_{-\phi_o}^{\phi_o} \frac{z\cos(\phi - \phi_1)\hat{\rho} - z\sin(\phi - \phi_1)\hat{\phi} + (-\rho\cos(\phi - \phi_1) + R)\hat{z}}{(R^2 + z^2 + \rho^2 - 2R\rho\cos(\phi - \phi_1))^{3/2}} d\phi_1$$

$$\overrightarrow{B_{st1}}(\rho, \phi, z) = \frac{\mu_o}{4\pi} NRI \int_0^{z_o} \frac{\sin(\phi_o - \phi)\hat{\rho} + (\rho - R\cos(\phi_o - \phi))\hat{\phi}}{(R^2 + \rho^2 - 2R\rho\cos(\phi_o - \phi) + (z - z_1)^2)^{3/2}} dz_1, \quad [1]$$

where $\mu_o = 4\pi \times 10^{-7}$ *henry/m* is the magnetic permeability of free space, N is the number of turns in each of the two coils, I is the current in the wire, and ρ, ϕ, and z are the standard cylindrical coordinates of the spatial point (being $\hat{\rho}$, $\hat{\phi}$, and $\hat{z}$ the corresponding unitary vectors). If the spatial magnitudes are given in millimeters (mm), I in Amperes (A), and the constant $\mu_o/4\pi$ is taken as the unitary, the magnetic field will be obtained directly in Gauss (G) ($1G = 10^{-4}T$). Henceforth, this convention will be used to express magnetic field magnitudes.

The magnetic field produced by the other arcs or strips can be obtained through an adequate rotation or translation of the coordinate system. The analytical final expression for the total magnetic field involves different elliptic integrals that can be evaluated numerically to obtain the desired field at a given spatial point.

To experimentally check the exact obtained expressions, a saddle coil with a 0.35-mm diameter wire and 50 turns was built. The geometric parameters were chosen to be $\phi_o = \pi/3$, $z_o = 220$ mm, and $R = 55$ mm; and the electric current was fixed to be $I = 2.5A$. The three magnetic field components (x, y, and z) were measured in 37 different spatial points in the central and the top planes of the coil, respectively. Magnetic field values for axial and transversal components were obtained using standard teslameters from Leybold Didactic GMBH, Hürth, Germany (model 51660/61/62). The sensitivity and the spatial resolution of both teslameters were estimated to be $1G$ (0.1 mT) and 8 mm^3 (4 mm^2 in the plane, and 2 mm in the z axis), respectively, during the whole experiment. To improve the accuracy in the determination of the spatial points, a suitable piece of wood was introduced inside the coil and 37 holes parallel to the axis of the coil system were made at the ϕ and ρ values where the magnetic field was going to be measured.

At a given spatial point, the value of each component of the magnetic field generated by the saddle coil system was obtained subtracting the measured value of the corresponding component *without* current (I) in the coils from the analogous measured value *with* current carried by the coils. The last procedure was performed with the purpose of discriminating between the magnetic field produced by the saddle coil and other irrevocably present magnetic fields (earth's field, for instance).

Analytical and experimental results are contrasted in Table 1. In this table, about 90% of the experimental data are indistinguishable from the analytically calculated values. This is a reasonably good agreement between both results, considering different experimental issues, such as a finite wire width or departures from the perfect geometry, that were not taken into account in the theoretical calculus. Greater differences between both values are mostly encountered at points where the magnetic field presents a strong spatial dependence.

Ideal Geometric Coil Configuration

The ideal geometric configuration of the saddle coil can be obtained from the analysis of the three components of the magnetic field uniformity.

A Taylor expansion of the three components of the magnetic field around the center of the coil $\vec{x_o}$ (the center of the sample as well) allows a direct evaluation of the field uniformity. According to that, if only the first four terms in the Taylor expansion are considered

$$B_i(\vec{x}) = B_i(\vec{x_o}) + T_{1i}(\vec{x}) + T_{2i}(\vec{x}) + T_{3i}(\vec{x}) + T_{4i}(\vec{x}) + O(x^5, y^5, z^5), \quad [2]$$

where $i = x, y, z$; $\vec{x} = (x, y, z)$; $\vec{x_o} = (0, 0, z_o/2)$, according to the coordinate system employed (see Fig. 1); $T_{ki}(\vec{x})$, ($k = 1, 2, 3, 4$) are the first-, second-, third-, and fourth-order terms in spatial variables of the i-th component of the magnetic field and $O(x^5, y^5, z^5)$ means terms higher than fourth order in spatial variables. In a general form, $T_{ki}(\vec{x})$ can be expressed as

Table 1 Experimental and Calculated Values of the Three Magnetic Field Components Generated by a Saddle Coil System with z_o = 220 mm, R = mm, $\phi_o = \pi/3$, I = 2.5A, N = 50 turns (A Good Agreement Is Observed, Taking into Account Experimental Errors ($\Delta = \pm 1G$). This Fact Makes Reliable the Exact Numerical Calculus.)

		Central Plane (z = 110 mm)						Top Plane (z = 220 mm)					
		Experimental Values (G) ($\pm 1G$)			Calculus Values (G)			Experimental Values (G) ($\pm 1G$)			Calculus Values (G)		
ϕ (rad)	ρ (mm)	B_x	B_y	B_z	B_x	B_y	B_z	B_x	B_y	B_z	B_x	B_y	B_z
0	0	16	0	0	16.5	0	0	8	0	0	7.9	0	0
0	14	16	0	0	15.4	0	0	7	0	−3	7.9	0	−4
0	29	16	0	0	15.7	0	0	7	1	−10	7.5	0	−9.8
0	44.5	12	0	0	13.5	0	0	6	0	−22	6.4	0	−24.6
π/6	19	16	0	0	16.6	0.2	0	8	1	−5	7.9	0.1	−4.9
π/6	34	17	2	0	16.7	1.7	0	8	0	−11	8.0	0.8	−11.6
π/6	49	13	4	0	14.9	5.2	0	7	2	−34	7.1	2.6	−37.6
π/3	10	16	0	0	16.5	0	0	8	0	−1	7.9	0	−1.4
π/3	25	15	0	0	16.9	−0.5	0	8	0	−3	8.1	−0.3	−4.0
π/3	40	20	−4	0	20.9	−3.8	0	10	−2	−10	10.0	−1.9	−9.0
π/2	15	16	1	0	16.4	0	0	8	0	0	7.8	0	0
π/2	30	14	1	0	15.0	0	0	7	−1	0	7.1	0	0
π/2	45	8	1	0	8.4	0	0	4	−1	0	3.9	0	0
2π/3	19	16	0	0	16.6	0.2	0	8	−1	2	7.9	0.1	2.8
2π/3	34	18	1	0	18.3	1.8	0	10	1	6	8.8	0.9	6.4
2π/3	49	29	11	0	35.4	13.1	0	16	7	17	17.3	6.5	19.2
5π/6	10	16	0	0	16.4	0	0	8	0	2	7.9	0	2.4
5π/6	26	16	−1	0	16.5	−0.6	0	7	−1	6	8.0	−0.3	7.4
5π/6	40	14	−2	0	16.4	−3.0	0	8	−2	16	7.9	−1.5	16.9
π	15	16	0	0	16.4	0	0	8	0	3	7.9	0	4.3
π	30	14	0	0	15.6	0	0	7	−1	8	7.4	0	10.4
π	45	14	1	0	13.4	0	0	6	0	22	6.3	0	25.6
7π/6	19	16	1	0	16.6	0.2	0	8	−1	5	7.9	0.1	4.9
7π/6	34	15	0	0	16.7	1.7	0	8	0	11	8.0	0.8	11.6
7π/6	49	15	7	0	14.9	5.2	0	8	2	34	7.1	2.6	37.6
4π/3	10	16	0	0	16.5	0	0	8	0	0	7.9	0	1.4
4π/3	25	16	0	0	16.9	−0.5	0	8	0	5	8.1	−0.3	4.0
4π/3	40	22	−2	0	20.9	−3.8	0	10	−3	9	10.1	−1.9	9.0
3π/2	15	16	−1	0	16.4	0	0	8	−1	0	7.8	0	0
3π/2	30	14	−1	0	15.0	0	0	7	0	0	7.1	0	0
3π/2	45	8	−1	0	8.4	0	0	4	−1	0	3.9	0	0
5π/3	19	16	0	0	16.6	0.2	0	8	0	−2	7.9	0	−2.8
5π/3	34	18	3	0	18.3	1.8	0	11	2	−6	8.8	0.9	−6.4
5π/3	49	39	10	0	35.4	13.1	0	16	8	−15	17.3	6.5	−19.2
11π/6	9	16	1	0	16.5	0	0	9	0	−3	7.9	0	−2.2
11π/6	25	15	−1	0	16.7	−0.5	0	8	0	−7	8.0	−0.3	−7.0
11π/6	40	15	−2	0	16.5	−3.0	0	8	0	−15	7.9	−1.5	−16.9

$$T_{ki} = \frac{1}{k!}\left[\sum_{k_1+k_2+k_3=k}^{k} \frac{k!}{k_1!k_2!k_3!}\, x^{k_1} y^{k_2}\left(z - \frac{z_o}{2}\right)^{k_3} \cdot \frac{\partial^k B_i}{\partial x^{k_1}\partial y^{k_2}\partial z^{k_3}}\bigg|_{\vec{x}_o}\right]. \quad [3]$$

In this way $T_{1i} = \partial B_i/\partial x|_{(0,0,z_o/2)}x + \partial B_i/\partial y|_{(0,0,z_o/2)}y + \partial B_i/\partial z|_{(0,0,z_o/2)}(z - (z_o/2))$ and so forth.

Note in Eq. [2] that to maximize uniformity around $\vec{x}_o$ (i.e., minimize $B_i(\vec{x}) - B_i(\vec{x}_o) = T_{1i}(\vec{x}) + T_{2i}(\vec{x}) + \ldots$), the terms of the Taylor expansion should be as small as possible. Consequently, the first

four terms of the Taylor expansion of the three components of the magnetic field were calculated.

The zero order term was

$$B_x(\vec{x_o}) = \frac{16IN(s-1)(s^{-1/2}+s^{-3/2})\sin(\phi_o)}{z_o}$$

$$B_y(\vec{x_o}) = B_z(\vec{x_o}) = 0, \qquad [4]$$

where $s = 1 + (z_o/2R)^2$. This last expression is in complete agreement with (*14*) (considering differences between both notations). The result is expressed in terms of z_o because R is usually constrained in NMR experiments. Because of symmetry reasons, B_x odd-order derivatives with respect to x, y, or z; B_y odd-order derivatives with respect to z or even-order derivatives with respect to x or y; and B_z odd-order derivatives with respect to y or even-order derivatives with respect to x or z are all null (no derivative is considered as a zero- [even] order derivative). Therefore, $T_{1i}(\vec{x}) = T_{3i}(\vec{x}) = 0$; $i = x, y, z$, and only a few derivatives survive. Second- and fourth-order derivatives were calculated to be

$$\left.\frac{\partial^2 B_x}{\partial x^2}\right|_{\vec{x_o}} = \frac{64IN(s-1)^2\sin(\phi_o)((-5-3s-4s^2-8s^3)\sin^2(\phi_o)+15+3s^2+6s^3)}{z_o^3 s^{7/2}}$$

$$\left.\frac{\partial^2 B_x}{\partial y^2}\right|_{\vec{x_o}} = \frac{-64IN(s-1)^2\sin(\phi_o)((-5-3s-4s^2-8s^3)\sin^2(\phi_o)+3s+3s^2+6s^3)}{z_o^3 s^{7/2}} = \left.\frac{\partial^2 B_y}{\partial x \partial y}\right|_{\vec{x_o}}$$

$$\left.\frac{\partial^2 B_x}{\partial z^2}\right|_{\vec{x_o}} = \frac{192IN(s-1)^2\sin(\phi_o)(s-5)}{z_o^3 s^{7/2}} = \left.\frac{\partial^2 B_z}{\partial x \partial z}\right|_{\vec{x_o}} \qquad [5]$$

$$\left.\frac{\partial^4 B_x}{\partial x^4}\right|_{\vec{x_o}} = \frac{768IN(s-1)^3\sin(\phi_o)(A\sin^4(\phi_o)+B\sin^2(\phi_o)+C)}{z_o^5 s^{11/2}}$$

$$\left.\frac{\partial^4 B_x}{\partial y^4}\right|_{\vec{x_o}} = \frac{768IN(s-1)^3\sin(\phi_o)(A\sin^4(\phi_o)+(B+210-70s)\sin^2(\phi_o)+C-10s^2+175s-315)}{z_o^5 s^{11/2}}$$

$$\left.\frac{\partial^4 B_x}{\partial z^4}\right|_{\vec{x_o}} = \frac{3840IN(s-1)^3\sin(\phi_o)(4s^2-49s+63)}{z_o^5 s^{11/2}}$$

$$\left.\frac{\partial^4 B_x}{\partial x^2 \partial z^2}\right|_{\vec{x_o}} = \frac{3840IN(s-1)^3((-7s+21)\sin^2(\phi_o)-3s^2+42s-63)}{z_o^5 s^{11/2}}$$

$$\left.\frac{\partial^4 B_x}{\partial y^2 \partial z^2}\right|_{\vec{x_o}} = -\frac{3840IN(s-1)^3((-7s+21)\sin^2(\phi_o)+s^2-7s)}{z_o^5 s^{11/2}}$$

$$\left.\frac{\partial^4 B_x}{\partial x^2 \partial y^2}\right|_{\vec{x_o}} = \frac{-768IN(s-1)^3\sin(\phi_o)(A\sin^4(\phi_o)+(B+105-35s)\sin^2(\phi_o)+C-15s^2+210s-315)}{z_o^5 s^{11/2}}$$

$$\left.\frac{\partial^4 B_y}{\partial x^3 \partial y}\right|_{\vec{x_o}} = \left.\frac{\partial^4 B_x}{\partial x^2 \partial y^2}\right|_{\vec{x_o}}; \quad \left.\frac{\partial^4 B_y}{\partial y^3 \partial x}\right|_{\vec{x_o}} = \left.\frac{\partial^4 B_x}{\partial y^4}\right|_{\vec{x_o}}; \quad \left.\frac{\partial^4 B_y}{\partial z^2 \partial x \partial y}\right|_{\vec{x_o}} = \left.\frac{\partial^4 B_x}{\partial y^2 \partial z^2}\right|_{\vec{x_o}}$$

$$\left.\frac{\partial^4 B_z}{\partial x^3 \partial z}\right|_{\vec{x_o}} = \left.\frac{\partial^4 B_x}{\partial x^2 \partial z^2}\right|_{\vec{x_o}}; \quad \left.\frac{\partial^4 B_z}{\partial z^3 \partial x}\right|_{\vec{x_o}} = \left.\frac{\partial^4 B_x}{\partial z^4}\right|_{\vec{x_o}}; \quad \left.\frac{\partial^4 B_z}{\partial y^2 \partial x \partial z}\right|_{\vec{x_o}} = \left.\frac{\partial^4 B_x}{\partial y^2 \partial z^2}\right|_{\vec{x_o}}, \qquad [6]$$

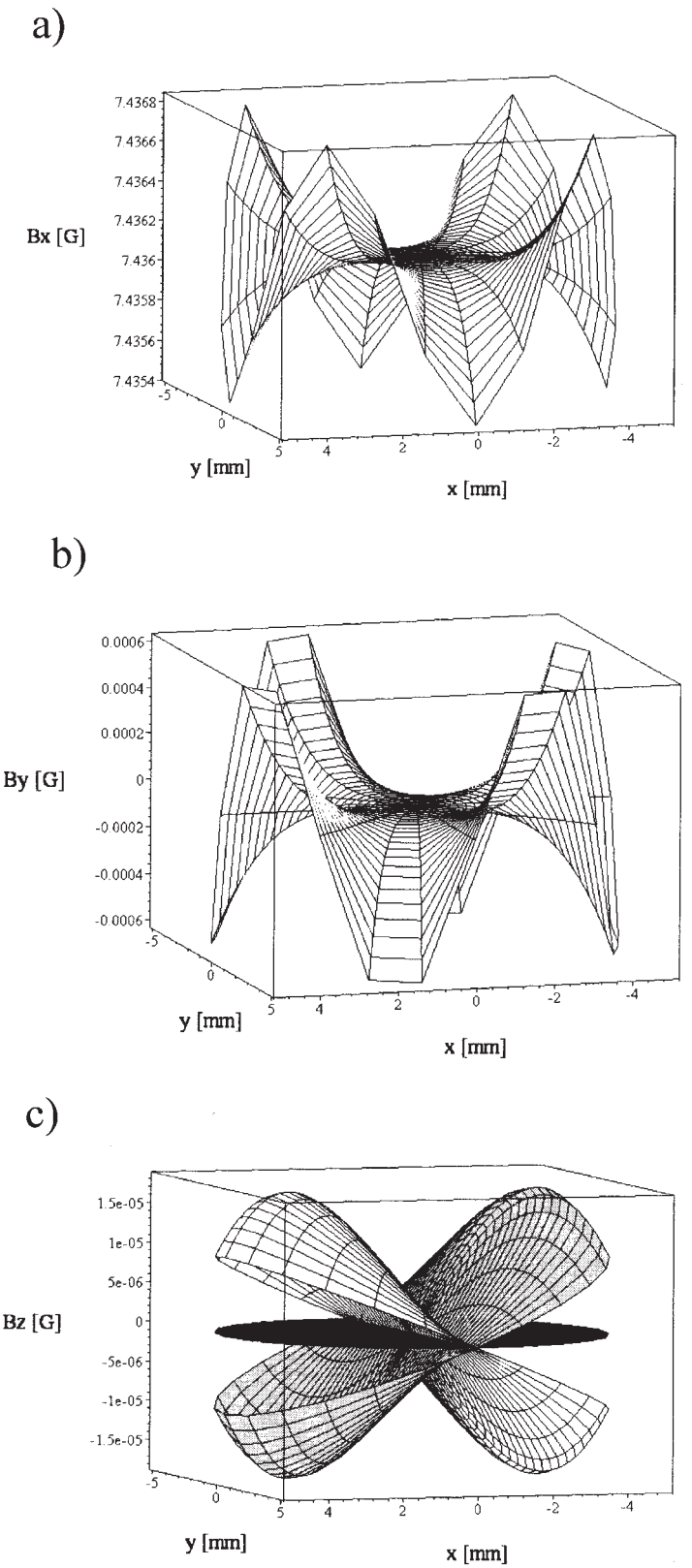

Figure 2 B_x (a) and B_y (b) magnetic-field-component values at the central plane of the sample for the optimum geometric configuration of the saddle coil system. Figure (c) shows the spatial dependence of the B_z magnetic field component for the central (black), top (grey), and bottom (white) planes of the sample. Typical sample dimensions were considered (l = 10 mm, d = 10 mm).

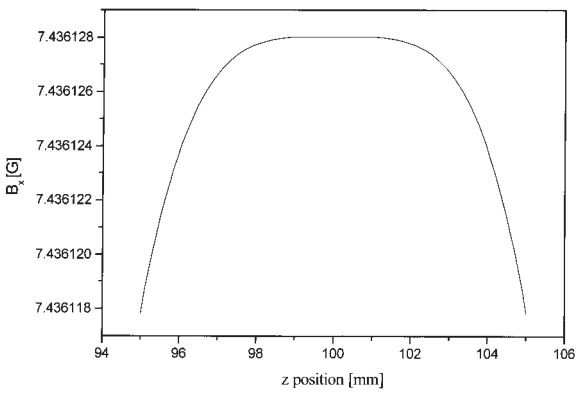

Figure 3 $B_x(z)$ dependence in the cylindrical axis of the sample for the optimum geometric configuration of the saddle coil system. Here, the magnetic field uniformity is clearly appreciated.

with

$$A \equiv 128s^5 + 64s^4 + 48s^3 + 40s^2 + 35s + 63$$

$$B \equiv -160s^5 - 80s^4 - 60s^3 - 50s^2 - 210$$

$$C \equiv 40s^5 + 20s^4 + 15s^3 + 25s^2 - 175s + 315. \quad [7]$$

Considering first the second-order derivatives (Eq. [5]) and, disregarding the trivial solutions such as $\phi_o = 0$ or $z_o = 0$ ($s = 1$), the only pair of parameters (ϕ_o, s) that cancel out all these derivatives is ($\phi_o = \pi/3$, $s = 5$ ($z_o = 4R$)), giving in this way the ideal geometric configuration for the saddle coil. This result agrees with (*14*), although B_y and B_z second-order derivatives were not considered in this reference.

To graphically appreciate the uniformity of the magnetic field produced by the ideally configured saddle coil, the three components of the magnetic field were calculated at the top, central, and bottom planes of a cylindrical NMR sample with typical dimensions: height $l = 10$ mm and diameter $d = 10$ mm. Figure 2 shows the values of the three magnetic field components for the central plane of the sample produced by a coil with $I = 1A$, $N = 50$, $z_o = 200$ mm, $R = 50$ mm. In case of B_z, the values in the three planes were included in the graph. In Fig. 3, the $B_x|_{x=y=0}$ dependence with coordinate z along the sample is shown. In this figure, the high uniformity of the field within the central region can be clearly appreciated.

For the optimum geometric configuration, the fourth-order Taylor expansions for the three components of the magnetic field can be easily calculated from Eq. [6]:

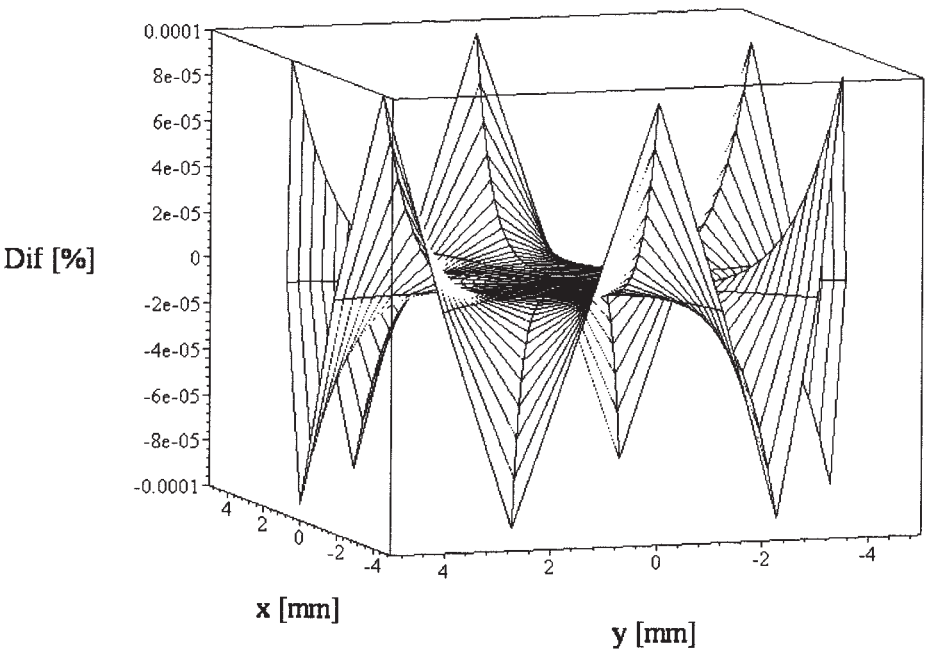

Figure 4 Percentile relative difference between exact values and fourth-order Taylor expansion for B_x magnetic field component at the top plane of the sample zone. Typical sample ($l = 10$ mm, $d = 10$ mm) and ideal saddle-coil geometric dimensions ($z_o = 200$ mm, $R = 50$ mm, $\phi_o = \pi/3$) were used.

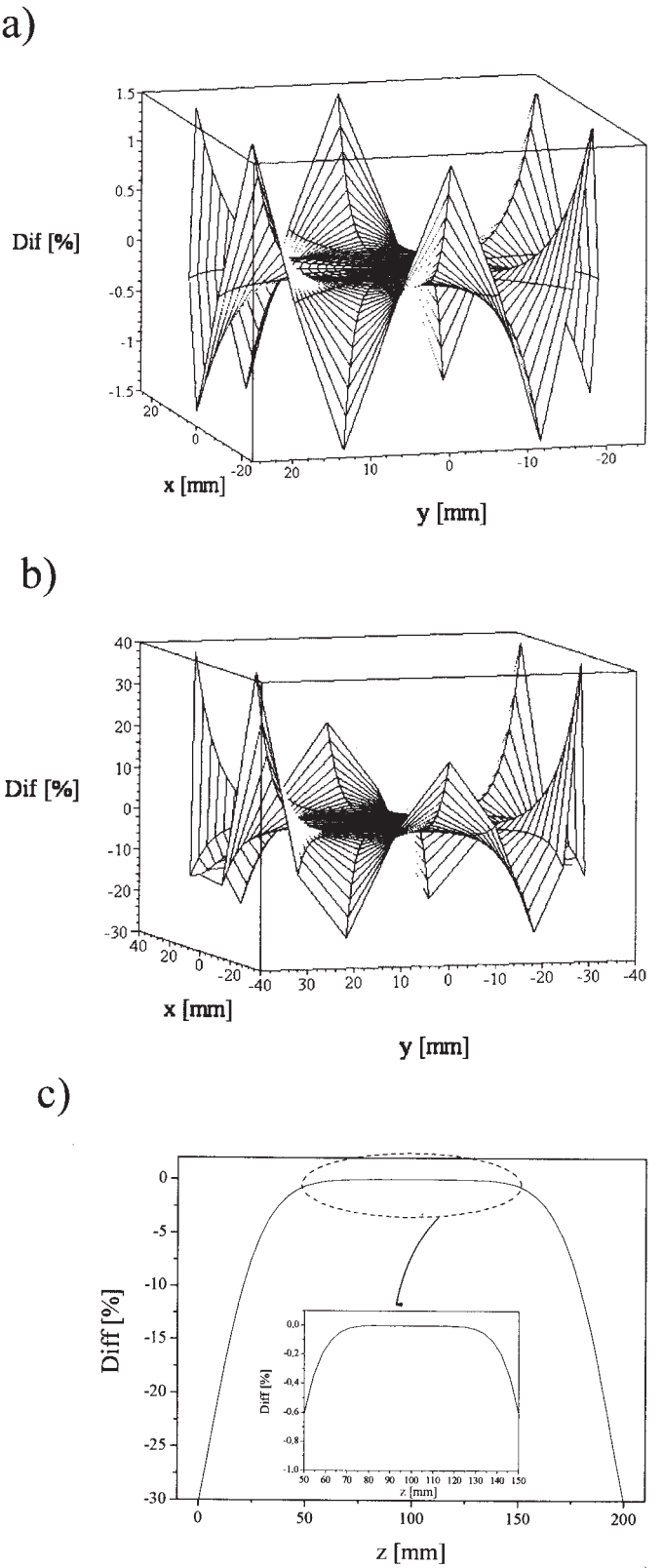

Figure 5 Percentile relative difference between B_x exact values and B_x fourth-order Taylor expansion for a saddle coil system with the optimum geometry. B_x magnetic field component at the central plane of the coil for $0 < \rho < 25$ mm ($R/2$) and for $0 < \rho < 40$ mm are considered in (a) and (b), respectively. Figure (c) shows the $B_x(z)$ dependence of this relative difference along the full cylindrical axis of the coil (external plot) and for $z_o/4 < z < 3z_o/4$ (internal plot). Sample and coil dimensions are the same as Fig. 4.

$$B_x(\vec{x}) - B_x(\vec{x_o}) \cong \frac{IN \times 10^2}{4! z_o^5} \left[-1700(x^4 + y^4 - 6x^2y^2) - 25\left(z - \frac{z_o}{2}\right)^4 + 114x^2\left(z - \frac{z_o}{2}\right)^2 + 37.2y^2\left(z - \frac{z_o}{2}\right)^2 \right]$$

$$B_y(\vec{x}) \cong \frac{IN \times 10^2}{4! z_o^5} \left[6800(x^3y - y^3x) + 74.4\left(z - \frac{z_o}{2}\right)^2 xy \right]$$

$$B_z(\vec{x}) \cong \frac{IN \times 10^2}{4! z_o^5} \left[-100\left(z - \frac{z_o}{2}\right)^3 x + 76x^3\left(z - \frac{z_o}{2}\right) + 74.4y^2x\left(z - \frac{z_o}{2}\right) \right] \quad [8]$$

Note that the field uniformity increases with z_o.

To check the Taylor expansions obtained, they were plotted as a function of spatial cylindrical coordinates ρ and ϕ for the top, central, and bottom sample planes and compared with the corresponding exactly calculated plots. In all cases, they present almost a complete agreement and a direct comparison between them can be appreciated in Fig. 4 for B_x at the top plane of the sample.

A spatially wider comparison between exact and fourth-order Taylor expansion can be observed in Fig. 5. In these figures, $Dif = B_x - Tay(Bx)/B_x(0, 0, z_o/2)$ represents the difference between exact values and fourth-order Taylor expansion in B_x, relative to the B_x value at the center of the coil system ($Tay(Bx)$ represents the fourth-order Taylor expansion). A noticeable agreement between them ($Dif < 1.5\%$) is appreciated when the central plane of the coil and distances minor than 25 mm ($R/2$) are considered (see Fig. 5[a]). However, departures from the exact result becomes important when 20 mm $< \rho <$ 40 mm (see Fig. 5). In Fig. 5(c) the dependence of Dif parameter with z coordinate is considered for the cylindrical axis of the coil. As it can be observed, $Dif <$ 1% when $|z - z_o/2| < z_o/4$. In these figures, coil and sample dimensions were the same as before. Analogous analyses were carried out for B_y and B_z components and no relevant differences were found in both cases.

Homogeneity Analysis of a General Geometric Coil Configuration

To quantify the relative homogeneity within the sample, parameter alpha is defined as

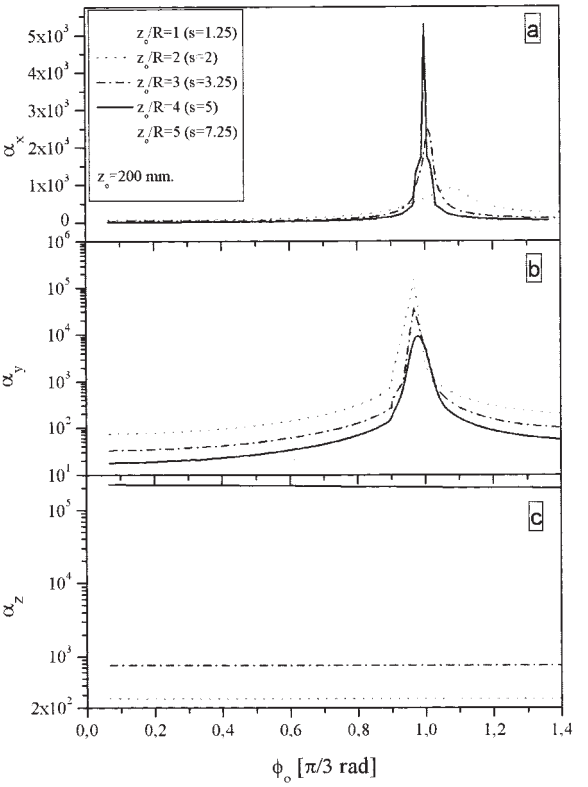

Figure 6 B_x (a), B_y (b), and B_z (c) relative homogeneities dependence on parameter ϕ_o within a sample with typical dimensions (l = 10 mm, d = 10 mm). Five different values of z_o/R ($1 \leq z_o/R \leq 5$) were considered. Parameter z_o was fixed to be 200 mm. Log scales were used for α_y and α_z plots, in order to appreciate the five curves.

$$\alpha_i = \left(\frac{B_i^{\max} - B_i^{\min}}{B_x(\vec{x_o})} \right)^{-1}, \quad [9]$$

where $i = x, y, z$; $B_i^{\max}$ and $B_i^{\min}$ are the maximum and minimum values of the i-th component of the magnetic field within the sample region, respectively. As defined in Eq. [9], α_i directly measures how homogeneous is the i-th component of the magnetic field in the sample region and will depend on the geometric parameters $\alpha_i = \alpha_i(\phi_o, s, z_o)$. Then, for a given set (ϕ_o, s, z_o) and given sample dimensions (l = 10 mm, d = 10 mm was used), α_i can be numerically calculated using exact or approximated expressions for $B_i(\vec{x})$.

Figure 6 shows the dependence of α_x, α_y, and α_z on ϕ_o, for a fixed value of z_o (z_o = 200 mm), and five different values of s parameter. As it can be observed in this figure, for a given s value, α_x and α_y present maximums at well-defined ϕ_o values (called ϕ_o^{opt}, henceforth). For s = 5, the maximums are obtained at $\phi_o^{opt} = \pi/3$ for both, α_x and α_y. Parameter

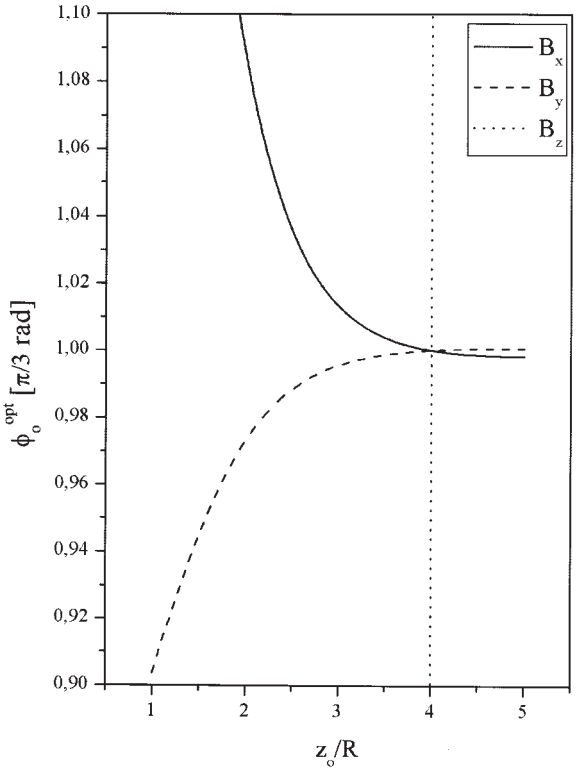

Figure 7 ϕ_o^{opt} (ϕ_o value at which α_i reaches its maximum) dependence on parameter z_o/R for B_x (solid line), B_y (dashed line), and B_z (dotted line) magnetic field components.

α_z shows an almost constant behavior with ϕ_o, $s = 5$ being the best configuration at a given ϕ_o value. These two facts clearly shows that ($s = 5$, $\phi_o = \pi/3$) is the optimum set of geometric parameters of a saddle-coil compensating system.

If the ideal geometric configuration cannot be achieved (because of experimental restrictions, for instance), it could be useful to know the ϕ_o^{opt} that gives maximum homogeneity for a given value of z_o/R (ϕ_o^{opt} only depends on s parameter). Figure 7 shows the dependence of ϕ_o^{opt} with z_o/R for the three components of the magnetic field. As it can be clearly appreciated in this figure, the maximum uniformity condition is simultaneously satisfied for the three components of the magnetic field, at the optimum geometric configuration. In addition, Table 2 numerically shows the dependence of ϕ_o^{opt} with z_o/R for the main component of the magnetic field, B_x.

Figures 6 and 7 are in complete agreement, and, in the previous analysis, we consider ϕ_o^{opt} as a function of z_o/R (instead of the opposite case) because in contrast with z_o/R, ϕ_o is not usually experimentally constrained.

DISCUSSION

The previous homogeneity study gives us the chance to easily evaluate how the compensating magnetic field produced by a saddle coil can influence in an NMR experiment. Typical magnetic field values to compensate in the x axis are of the order of 1 Gauss (the value of the Earth's magnetic field, approximately) and regular values of $z_o = 200$ mm and $R = 50$ mm were used for the dimensions of the coil. In this case, the maximum variation of the three components of the magnetic field within the sample region were

$$|B_x^{\max} - B_x^{\min}| \cong 1.8 \times 10^{-4} G \cong 0.76 \text{ Hz}$$
$$|B_y^{\max} - B_y^{\min}| \cong 1.5 \times 10^{-4} G \cong 0.65 \text{ Hz}$$
$$|B_z^{\max} - B_z^{\min}| \cong 5 \times 10^{-6} G \cong 0.022 \text{ Hz}. \quad [10]$$

In the last member of these equations, the magnetic field values are expressed in their equivalent proton Larmor frequency units.

Table 2 ϕ_o^{opt} Values at 40 Different Values of z_o/R Parameter for the B_x Magnetic Field Component (Main Component) (This Table Is Useful When the Optimum z_o/R Condition ($z_o/R = 4$) Cannot Be Fulfilled because of Experimental Restrictions.)

z_o/R	ϕ_o^{opt} (rad)	z_o/R	ϕ_o^{opt} (rad)	z_o/R	ϕ_o^{opt} (rad)	z_o/R	ϕ_o^{opt} (rad)
1.1	1.5444	2.1	1.1237	3.1	1.0583	4.1	1.0468
1.2	1.4081	2.2	1.1114	3.2	1.0560	4.2	1.0464
1.3	1.3437	2.3	1.1010	3.3	1.0541	4.3	1.0462
1.4	2.2957	2.4	1.0921	3.4	1.0525	4.4	1.0460
1.5	1.2571	2.5	1.0845	3.5	1.0511	4.5	1.0458
1.6	1.2249	2.6	1.0781	3.6	1.0500	4.6	1.0457
1.7	1.1978	2.7	1.0727	3.7	1.0491	4.7	1.0456
1.8	1.1747	2.8	1.0681	3.8	1.0483	4.8	1.0455
1.9	1.1550	2.9	1.0643	3.9	1.0477	4.9	1.0454
2.0	1.1381	3.0	1.0610	4.0	1.0472 (π/3)	5.0	1.0454

At high magnetic-field NMR, such deviations in the magnetic field produced by the saddle coil system itself are not relevant. However, such variations may become important in zero-field experiments and NMR field-cycling relaxometry. Typically, a field-cycling air magnet core presents a relative field homogeneity of 10^{-4} within the sample. Thus, changes introduced in B_z by the saddle coil will remain smaller or of the order of the magnet field inhomogeneities only if the proton Larmor frequency is higher or about 1 kHz.

Transversal components of the magnetic field are important in field-cycling experiments in the low-kilohertz frequency regime (even more when switching to zero field) (*12*). However, local field values in nonliquid samples are usually much bigger than the transversal variations encountered in the saddle coil magnetic field.

If the uniformity of the saddle-compensating coils needs to be increased for a particular experiment, and no experimental restrictions are present, the z_o and R values should be properly enlarged (keeping the optimum value $z_o/R = 4$). Naturally, the value of the current I and/or the number of turns N must be increased to compensate for the same magnetic field as before.

In case the homogeneity requirements of a particular experiment cannot be achieved with the saddle coil system analyzed, an appropriate higher-order shimming coil system could be implemented.

ACKNOWLEDGMENTS

F.B. acknowledges Conicet for their economic support (postdoctoral fellowship). E.A. is fellow of Conicet. Financial support from Fundación Antorchas, CONICET, and Secyt-UNC is acknowledged. Support from Ministero degli Affari Esteri (Italia) is also acknowledged.

REFERENCES

1. Garret MW. 1951. Axially symmetric systems for generating and measuring magnetic fiels. J Appl Phys 22:1091–1107.
2. Golay MJE. 1958. Field homogenizing coils for nuclear spin resonance instrumentation. Rev Sci Instrum 29: 313–315.
3. Anderson WA. 1961. Electrical current shims for correcting magnetic fields. Rev Sci Instrum 32:241–250.
4. Garret MW, Pissanetzsky S. 1971. Polygonal coil systems for magnetic fields with homogeneity of the fourth to the eighth order. Rev Sci Instrum 42:840–857.
5. Romeo F, Hoult DI. 1984. Magnetic field profiling: analysis and correcting coil design. Magn Reson Med 1:44–65.
6. Chmurny GN, Hoult DI. 1990. The ancient and honourable art of shimming. Concepts Magn Reson 2:131–149.
7. Hoult DI, Deslauriers R. 1994. Accurate shim-coil design and magnet-field profiling by a power-minimization-matrix method. J Magn Reson 108:9–20.
8. Konzbul P, Sveda K. 1995. Shim coils for NMR and MRI solenoid magnets. Meas Sci Technol 6:1116–1123.
9. Crozier S, Dodd, S, Doddrell DM. 1996. A novel design methodology for Nth order, shielded longitudinal coils for NMR. Meas Sci Technol 7:36–41.
10. Forbes LK, Crozier S. 2003. A novel target-field method for magnetic resonance shim coils: III. Shielded zonal and tesseral coils. J Phys D Appl Phys 36:68–80.
11. Anoardo E, Galli G, Ferrante G. 2001. Fast-field-cycling NMR: applications and instrumentation. Appl Magn Reson 20:365–404.
12. Anoardo E, Ferrante G. 2003. Magnetic field compensation for field-cycling NMR relaxometry in the ULF band. Appl Magn Reson 24:85–96.
13. Kimmich R, Anoardo E. 2004. Field-cycling NMR relaxometry. Prog Nucl Magn Reson Spectrosc 44:257–320.
14. Ginsberg DM, Melchner MJ. 1970. Optimum geometry of saddle shaped coils for generating a uniform magnetic field. Rev Sci Instrum 41:122–123.
15. Hoult DI, Richards RE. 1975. VHF FET preamplifier with 0.3 dB noise figure. Electron Lett 11:596–597.
16. Bottomley P. 1981. Digital gradient magnetic field reorientation in three-dimensional NMR zeugmatography. J Phys [E] 14:1052–1053.
17. Jackson JD. 1975. Classical electrodynamics. 2nd edition. New York: Wiley p 169–173.